Ron, H., Nowaczyk, N., Frank, U., Schwab, M. J., Naumann, R., Striewski, B., Agnon, A. (2007): Greigite detected as dominating remanence carrier in Late Pleistocene sediments, Lisan formation, from Lake Kinneret (Sea of Galilee), Israel. - Geophysical Journal International, 170, 1, pp. 117—131.

DOI: http://doi.org/10.1111/j.1365-246X.2007.03425.x

Geophys. J. Int. (2007) **170,** 117–131 doi: 10.1111/j.1365-246X.2007.03425.x

Greigite detected as dominating remanence carrier in Late Pleistocene sediments, Lisan formation, from Lake Kinneret (Sea of Galilee), Israel

H. Ron,[1,2] N. R. Nowaczyk,[3] U. Frank,[3] M. J. Schwab,[3] R. Naumann,[4] B. Striewski[3,5] and A. Agnon[1]

[1] *Institute of Earth Sciences, The Hebrew University, Givat Ram, Jerusalem* 91904*, Israel. E-mail: hagairon@vms.huji.ac.il*
[2] *Western Galilee College, Acre,* 24121 *Israel*
[3] *GeoForschungsZentrum Potsdam, Section* 3.3*, Telegrafenberg,* D-14473*, Potsdam, Germany*
[4] *GeoForschungsZentrum Potsdam, Section* 4.2*, Telegrafenberg,* D-14473*, Potsdam, Germany*
[5] *Massey University, Palmerston North, New Zealand*

Accepted 2007 March 2. Received 2007 March 2; in original form 2006 March 20

SUMMARY

A rock magnetic investigation of three sedimentary cores of Lisan formation of late Pleistocene age from Lake Kinneret (Sea of Galilee) northern Israel demonstrates that the magnetization of these sediments is controlled by various degrees of a secondary chemical remanent magnetization (CRM) carried by greigite (Fe_3S_4). This CRM is superimposed on a primary detrital remanent magnetization (DRM) that resides in Ti-magnetite. This finding is independently confirmed by X-ray diffraction (XRD) measurements performed on magnetic extracts of the sediments. The domain state of the greigite is largely single domain behaviour (SD), thus dominating the magnetization. Therefore, the magnetic record retrieve from of these sediments is not reflecting geomagnetic variations but rather chemical rock magnetic properties, resulting from diagenetic processes.

The results of our study suggest that paleomagnetic record of greigite bearing sediments should be interpreted with caution because of the following reasons:

1. Geomagnetic secular variations can be biased, due to large coercivity overlap between magnetite and greigite.
2. Alternating field (AF) demagnetization can produce erroneous directions due to vector distortion by acquisition of a gyro-remnant magnetization (GRM).
3. Estimation of relative paleointensity can be hampered by large-scale variations in natural remnant magnetization (NRM) intensity, caused by the acquisition of a secondary CRM of unknown age and unknown extent superimposed on the DRM.

The precipitation of greigite requires reducing conditions at the sediment–water interface and/or interstitial water, associated with the presence of sulphur and iron oxides. Reducing conditions are typical of stratified lakes and other stratified water bodies, such as the Dead Sea, paleo-Lake Lisan, temporarily the Eastern Mediterranean Sea, the Caspian Sea, the Black Sea and many other marine basins. According to our findings, paleomagnetic records from such environments carried dominantly by greigite therefore should be treated with care.

Key words: chemical remanent magnetization, geomagnetic secular variations, lake sediments, magnetostratigraphy, palaeomagnetism, rock magnetism.

INTRODUCTION

The origin of the Earth magnetic field and the ability to model its past behaviour, remain among the outstanding challenges of Earth sciences. Therefore, the study and documentation of geomagnetic field behaviour became the focus of many studies during the last 30 yr or so. A large part of the known world record was obtained from sequences of oceanic and lake sediments, with each of these environments having its advantages and disadvantages. Lacustrine sequences are frequently used to study geomagnetic field variations because they are rapidly deposited and they are relatively easy to date using radiocarbon and U-series methods (e.g. Kawai *et al.* 1975; King *et al.* 1983; Thouveny *et al.* 1993; Tauxe 1993; Creer & Morris 1996; Peck *et al.* 1996; Williams *et al.* 1998; Marco *et al.*

1998; Burchfield & Banerjee 2000; Frank *et al.* 2002; Nowaczyk *et al.* 2002). Therefore, on principle, high-resolution directional and paleointensity records of paleosecular variations (PSV) can be ideally obtained. However, these expectations require that the magnetization is a detrital remanent magnetization (DRM) and has remained so ever since sediment deposition. This last condition is crucial since diagenesis and chemical alteration is prevailing in many lacustrine and marine depositional environments and can completely alter the original DRM and/or add a new secondary chemical remanent magnetization (CRM), generally growing with an unknown time lag and unknown duration.

There is growing evidence that the magnetic recording process in lake sediments is strongly influenced by environmental conditions in the catchments area and in the depositional basin. Important among these conditions are variations in grain size and post-depositional diagenetic processes (Nowaczyk 2001 and references therein). Both processes affect the fidelity of the sediments as a recorder of the ancient field direction and relative paleointensity.

In the present study, we report a rock magnetic study of three sedimentary cores of the late Pleistocene Lisan formation from Lake Kinneret (Sea of Galilee), northern Israel. These cores, spanning the time interval from about 40 to 20ka, demonstrate that the magnetization of the recovered sediments is largely controlled by various degrees of a greigite-carried CRM superimposed on, and biasing the primary DRM carried by Ti-magnetite. Thus the natural remnant magnetization (NRM) record is mostly controlled by chemical processes and not by geomagnetic field variations.

DRY LAKE LISAN SEDIMENT

The Lisan Formation was deposited in Lake Lisan, the precursors of the modern Dead Sea and Sea of Galilee. The formation is widely exposed in the Jordan — Dead Sea rift valley, from south of the Dead Sea to the Sea of Galilee in the north. It appears that the water bodies, occupying the Dead Sea — Jordan rift valley during the late Pleistocene, were separated for most of the past 70 kyr, the last Glacial and the Holocene, and merged into a single lake only for a short interval of time, around the glacial maximum between 26–24 kyr BP (Bartov *et al.* 2002; Hazan *et al.* 2005).

After this episode, Lake Lisan began to retreat at ∼17–15 kyr cal BP (Begin *et al.* 1985; Bartov *et al.* 2002), and reached its minimum stand at ∼13–12 kyr (Stein 2001). Whereas, lake Kinneret has remained a flow through fresh water body, the Dead Sea became a terminal hyper saline water body. The two remnants of Lake Lisan at its maximum level are the modern Dead Sea and Lake Kinneret.

We studied the paleomagnetism and rock magnetic properties of nine meters of the Lisan Formation via three cores spanning the time interval from about 40 to 20 ka in the southern part of the Sea of Galilee (Fig. 1).

PREVIOUS PALEOMAGNETIC STUDIES ALONG THE DEAD SEA RIFT

Both the Lisan and Kinneret formations were the target of several paleomagnetic studies during the last 20 yr. Thompson *et al.* (1984) studied two Holocene sedimentary cores and provided a paleosecular variation (PSV) curve for the last 6 ka. Since no rock magnetic data were presented, it appears that they *a priori* assume that the magnetization is a primary DRM. Marco *et al.* (1998) and Marco *et al.* (1999) studied the paleomagnetism and rock magnetism of the laminated Lisan Formation at Perazim Valley, southern Dead Sea region. They demonstrate that magnetizations are of DRM origin and limited to the dark detrital laminas, whereas the bright aragonitic laminas are nearly non-magnetic: they infer a ca. 40 kyr directional

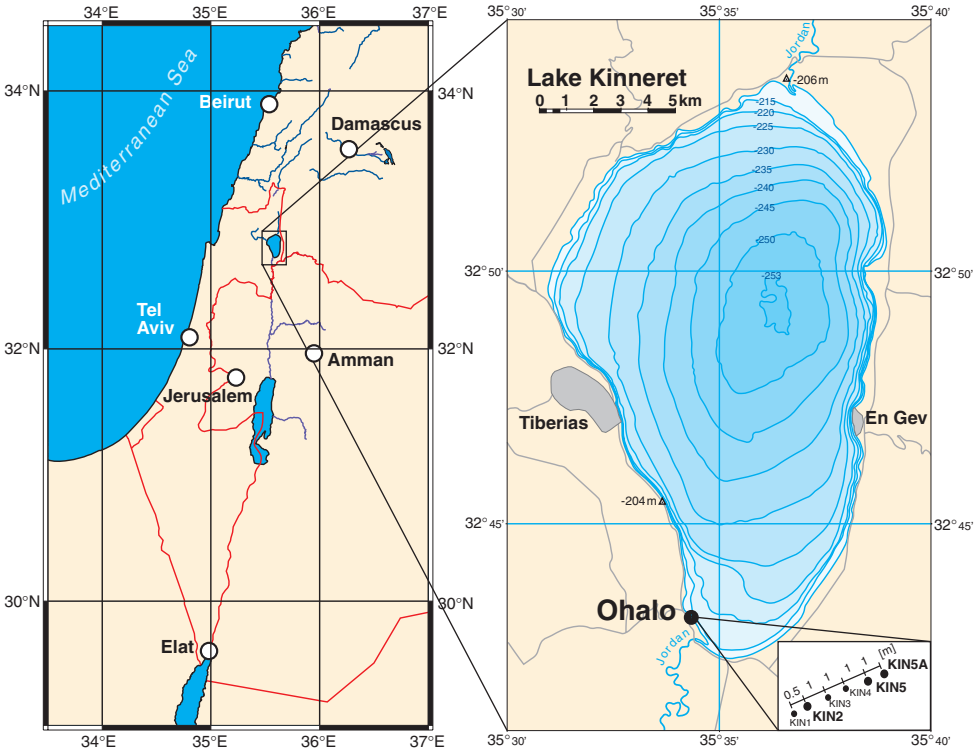

Figure 1. Location map of Lake Kinneret in Israel and the coring sites at the southwestern shore.

PSV curve, including evidence for the Laschamp geomagnetic excursion. However, a relative paleointensity record could not be obtained. Ron *et al.* (2006) studied the rock magnetism of Lisan and Ze'elim Formations (Dead Sea region) in some detail. They reported that the magnetization of Holocene Dead Sea sediments is of CRM origin (Ze'elim Formation) dominated by greigite, and overwhelming the DRM. They demonstrate that the fresh Lisan sediments at the lower part of the exposed section are also containing various amounts of greigite and that a reliable geomagnetic record can be obtained only from Lisan sediments sequence above this lower part. Ron *et al.* (2006) conclude that the Lisan formation failed to provide a relative paleointensity record because the primary DRM first has been altered by dissolution of fine-grained Ti-magnetite along with formation of greigite under anoxic conditions. And second, after retreat of the water and exposure of the sediments to air the greigiet was oxidized to non-magnetic phases, leaving only the coarse-grain PSD and MD Ti-magnetite, that enable to recover directional record only.

Marco (2002) studied the PSV of a 4 m thick lake sediment sequence at Ohalo-II archaeological site, southern Sea of Galilee (Fig. 1). Having no rock magnetic data, he assumed that magnetization was a stable, primary DRM. The calibrated radiocarbon age at the site is 22–23 ky. Marco (2002) reported anomalous directions at about 2.5 m below the surface, he imported the depth–age model of the Lisan formation from the Dead Sea area to Ohalo section and concluded that the anomalous direction directions correspond to the Mono Lake excursion.

Frank *et al.* (2002; 2003) studied the paleo- and rock-magnetism of the Late Holocene sedimentary sequence of Birkat Ram volcanic crater lake, 50 km north of Lake Kinneret. They infer records of relative paleointensity variations as well as directional PSV records for the last 6.4 ka according to a new depth–age model by Schwab *et al.* (2004).

MATERIALS AND METHODS

Coring and sampling

During a field campaign in 1999, a total of six cores was retrieved along transect on-shore Lake Kinneret, deploying a modified GFZ Usinger piston-coring system. The present study focuses on three sediment cores of up to 885 cm length. Two different core diameters, 80 and 57 mm, respectively, were used, depending on nature of the sediment. The individual 1 and 2 m long core-sections of drill holes KIN2, KIN5 and KIN5A (Figs. 1 and 2) were cut into 1 m sections, split into working and archive halves, sealed in plastic tubes, and stored in a cooled room at 4°C. For the three different sites, continuous composite profiles were compiled from the individual overlapping cores, using magnetic susceptibility (see below) and lithology (Fig. 2). For paleo- and rock-magnetic investigations the cores were sampled with 6 cm^3 plastic cubes at a uniform interval.

Lithology

The lithology of the studied cores is shown in Fig. 2. The recovered sequence is composed of mainly laminated and massive sediments. Laminas are composed of clay and silt, alternating with calcite. The massive sediments contain a mixture of varying amount of silt and clay. The lithology dissimilarities (Fig. 2) of the upper 2–3 m within the core transect, when combined with the age data, suggest that a correlation of the individual cores is not trivial, even though the horizontal distance between the cores is only 4 m. The only three AMS ^{14}C ages data also suggest that correlation is not trivial.

Age dating

The sedimentary sequence of the cores belongs to the upper part of Lisan formation (Hazan *et al.* 2005). Three radiocarbon (^{14}C) measurements were carried out using Accelerator Mass Spectrometry, at the Leibniz Laboratory, Kiel (KIA), Germany. Two *Melanopsis* (fresh water gastropod) samples for radiocarbon dating were taken from core KIN2and a coal chunk from KIN5A. Core KIN2 was sampled at 880 cm (KIN2-6B/KIA14369) and 230 cm (KIN2-3A-2/KIA14372), respectively, and the sample from core KIN5A was taken at 260 cm (KIN5-2B-3/KIA14370, Fig. 2). The ^{14}C ages of 880 cm, 230 cm (core KIN2) and 260 cm (core KIN5A) are 40.5, 21.4 and 33.0 ky, respectively, and calibrated ages are 41.5, 23.0 and 35.0 ky (for calibration, see Hazan *et al.* 2005). This set of radiocarbon ages is therefore insufficient to establish a clear stratigraphic and chronological correlation between the two cores.

High-resolution logging of magnetic susceptibility

High-resolution determination of magnetic susceptibility was performed on the archive halves of the core sections using an automated logging system, developed at the GFZ Potsdam, in combination with a Bartington MS2E/1 spot-reading sensor. The bell-shaped response function of the sensor with respect to a thin magnetic layer has a half-width of 3.5 mm (Nowaczyk 2001), thus two thin magnetic layers; about 4 mm apart can be resolved with this sensor. Measurements were performed at 1 mm increments with calibration readings against air every 10 measurements in order to monitor the thermally induced drift of the susceptibility sensor. This drift was subsequently subtracted from the readings, which were then multiplied with an empirically determined calibration factor of 8.9 in order to yield correct volume susceptibility values as multiples of 10^{-6}.

Anisotropy of magnetic susceptibility (AMS)

The anisotropy ellipsoid of magnetic susceptibility was determined on the cubic paleomagnetic samples using an AGICO KLY-3S. During analysis, susceptibility is numerously measured while the sample is rotating around the *x*-, *y*- and *z*-axis, respectively. This is done after zeroing the instrument with the sample inside the measuring coil. This means that during rotation, only the deviation of the ellipsoid from a sphere is determined so that the most sensitive range can be used in most cases. Absolute values of the susceptibility anisotropy ellipsoid are then determined from an additional bulk measurement. Calculation of the anisotropy tensor, represented by the principal susceptibilities axis K_{max} (maximum), K_{int} (intermediate) and K_{min} (minimum), and their respective orientation angles, declination (D) and inclination (I), was then performed with AGICO software (Brno, Czech Republic). Since the core is non-oriented, the orientation angles are given with respect to sample coordinates where *x* and *y* axes are the horizontal plane and *z* the vertical (core) axis. For the degree of AMS, the ratio $100(K_{max}-K_{min})/K_{max}$ is used and is therefore given as percentage, whereas the shape of the ellipsoid is estimated by (factor) $(K_{max}-K_{min})/K_{int}^2$, with values <1 (>1) indicating an oblate (prolate) ellipsoid. (e.g. Nowaczyk 2003).

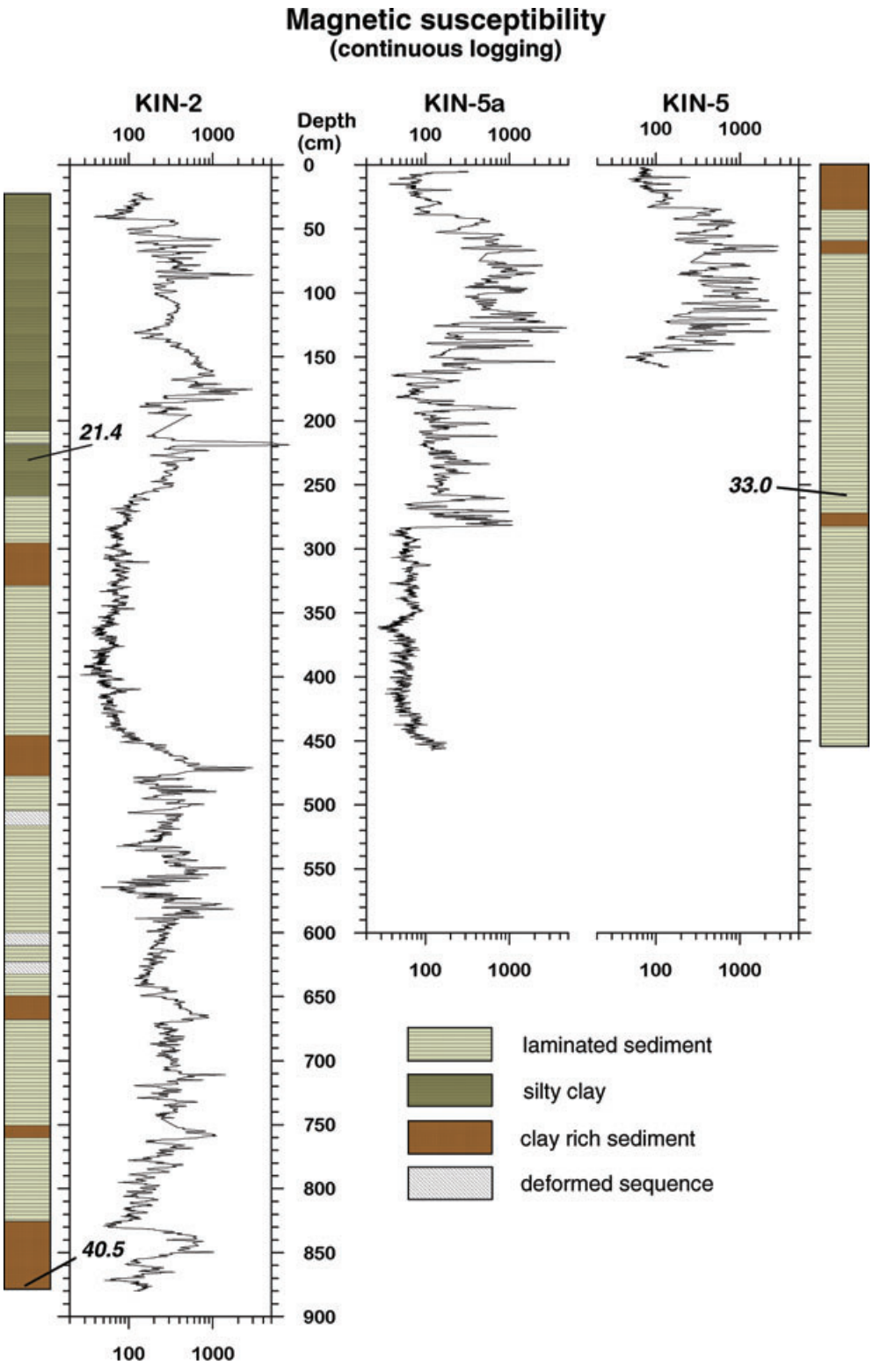

Figure 2. Simplified lithology and high-resolution records of the magnetic susceptibility of cores KIN2 and KIN5 measured on the split surfaces of the cores and radiocarbon ages (ka). For methodological explanation see text.

NRM demagnetization

Measurements and demagnetization of the natural remanent magnetization (NRM) and anhysteretic remanent magnetization (ARM) were performed on the discrete samples with a fully automated 2G ENTERPRISES DC-SQUID 755 SRM long-core system with an in-line tri-axial alternating field (AF) demagnetizer. All samples were demagnetized in 8 to 10 steps with maximum AF amplitude of 80 mT or up to 100 mT when required. The characteristic remanent magnetization (ChRM) of each sample was then determined by

subjecting its demagnetization results to principal component analysis (Kirschvink 1980). The median destructive field of the NRM (MDF_{NRM}) was automatically determined for each sample as a first estimate of the remanence coercivity of the investigated sediments.

ARM acquisition

Acquisition of ARM as measures of concentration of magnetic minerals was performed along the sample's positive *z*-axis with 0.05 mT static field and 100 mT AF amplitude. The ARM was also measured with the cryogenic magnetometer and demagnetized at the same AF levels that were used for NRM demagnetization (up to 65 mT). The MDF of ARM (MDF_{ARM}) was calculated for comparison with the MDF_{NRM}. Besides the coercivity spectrum, directional effects also influence the shape of the NRM demagnetization curve. That is, vectors of different direction and of stability are superimposed and affect the decay of the absolute NRM intensity and probably the MDF_{NRM}. In contrast, the decay of the uni-vectorial ARM during demagnetization is influenced by the coercivity spectrum alone. The anhysteretic susceptibility κ_{ARM} was also calculated. It is defined as the ARM intensity normalized by the static field amplitude used in the ARM acquisition process, here 0.05 mT.

IRM acquisition

Isothermal remanent magnetizations (IRM) were imprinted with a pulse magnetizer (2G Enterprises 660) and measured with a Molyneux fluxgate spinner magnetometer (Minispin), since IRM intensities often exceed the sensitivity range of the cryogenic magnetometer. All samples were exposed to a peak field of 1500 mT along their positive *z*-axis. The IRM acquired at 1500 mT is defined as 'saturation' isothermal remanence (SIRM). Afterwards, the samples were exposed to a field of −300 mT in opposite direction. The *S*-ratios, defined as $S = 0.5[1-(IRM_{-0.3T}/IRM_{1.8T})]$, with $S = 1$ for 100 percent magnetite and/or greigite, and $S = 0$ for 0 percent magnetite/greigite and 100 percent high-coercivity minerals, such as hematite and/or goethite. The ratio of SIRM to low-field susceptibility κ_{LF} was calculated in order to detect greigite bearing intervals, which are, according to Roberts (1995) and Maher *et al.* (1999), characterized by high $SIRM/\kappa_{LF}$ ratios such as above 30 kAm^{-1}.

Thermomagnetic measurements with VFTB

A fully computer controlled 'Variable Field Translation Balance' (VFTB) was used for obtaining thermomagnetic curves between room temperature and 700°C. The VFTB combines the principles of a classical horizontal Curie balance and an alternating gradient force magnetometer, for details see Nowaczyk *et al.* (2000). For measurements, about 0.1 cm^3 of fresh material was taken from the paleomagnetic samples. In some cases, different layers from within one sample box where analyzed, since it became obvious, that in Lake Kinneret sediments, greigite is concentrated in distinct, dark greenish brown layers.

Hysteresis parameters and IRM acquisition with MicroMag

Approximately 15 mm^3 of sediment from selected samples was mixed together with non-magnetic cement to produce small pellets as samples for hysteresis parameters measurements using Princeton Measurements alternating gradient force magnetometer ($MicroMag^{TM}$). The maximum magnetic field for hysteresis loops was set to ±1T. The hysteresis parameters, saturation remanence (M_{SR}), saturation magnetization (M_S) and coercive force (B_C), were corrected for the high-field slope of the magnetization curves. Remanence coercivity (B_{CR}) was determined during separate backfield measurements with 1 T saturation field with increments of 3.5 mT during the reversed field of up to 70 mT (e.g. Nowaczyk *et al.* 2002). The $MicroMag^{TM}$ was used also for automated IRM acquisition experiments using equal steps on a logarithmic axis, all together total of 60 steps from 2 to 2200 mT. The acquisition rate values were then calculated as $DJ_{IRM}/Dlog(B)$.

XRD of magnetic extract

From four intervals in Core KIN5A (Table 1), larger amounts of sediment were taken and dispersed in alcohol in an ultrasonic bath for about 15 min. A strong hand-held magnet, with a soft iron finger covered with a teflon hose was used in order to extract the magnetic fraction from the slurry. This was repeated three to four times per sample. We used a Siemens D5000 $\theta-2\,\theta$ powder diffractometer with Cu Kα radiation, automatic divergent and antiscatter slits and a secondary graphite monochromator with a scintillation counter. The diffraction data were recorded from 4 to 75° 2θ with a step width of 0.02° and a counting time of 4 sec./step. The generator settings were 40 KV and 30 mA. The Rietveld algorithm BGMN was used for quantitative analysis (Bergmann *et al.* 1998).

A complementary independent thermomagnetic experiment was performed on each sample using the VFTB (see above) to test the correlation between the results of the two methods.

Table 1. Main mineral contents and estimated errors (in per cent) of magnetic extracts from Core KIN5A, as derived from XRD analyses.

	Sample 1	Sample 2	Sample 3	Sample 4
Depth in core	113.0–118.0 cm	136.0–138.0 cm	140.0–102.0 cm	152.0–154.0 cm
Composite depth	97.7–100.4 cm	108.0–108.9 cm	109.8–110.7 cm	114.9–115.8 cm
Calcite	**36.50 ± 3.00**	**42.00 ± 3.00**	**25.10 ± 3.30**	**41.81 ± 2.97**
Greigite	**19.66 ± 1.50**	**23.98 ± 1.77**	**23.65 ± 1.83**	**13.97 ± 1.26**
Gypsum	**11.31 ± 2.88**			
Magnetite	**1.88 ± 0.84**		**2.68 ± 1.02**	**3.73 ± 3.73**
Ti-Magnetite		**3.81 ± 1.08**		
Pyrite	**6.95 ± 1.23**	**4.30 ± 1.08**	**25.73 ± 2.10**	**7.77 ± 1.11**
Quartz	**7.97 ± 1.47**	**13.10 ± 1.83**	**7.52 ± 1.68**	**9.67 ± 1.71**
Sulfur alpha	**15.80 ± 3.30**	**12.90 ± 3.60**	**15.30 ± 3.90**	**17.90 ± 3.30**
Lepidocrocite				**5.18 ± 1.14**

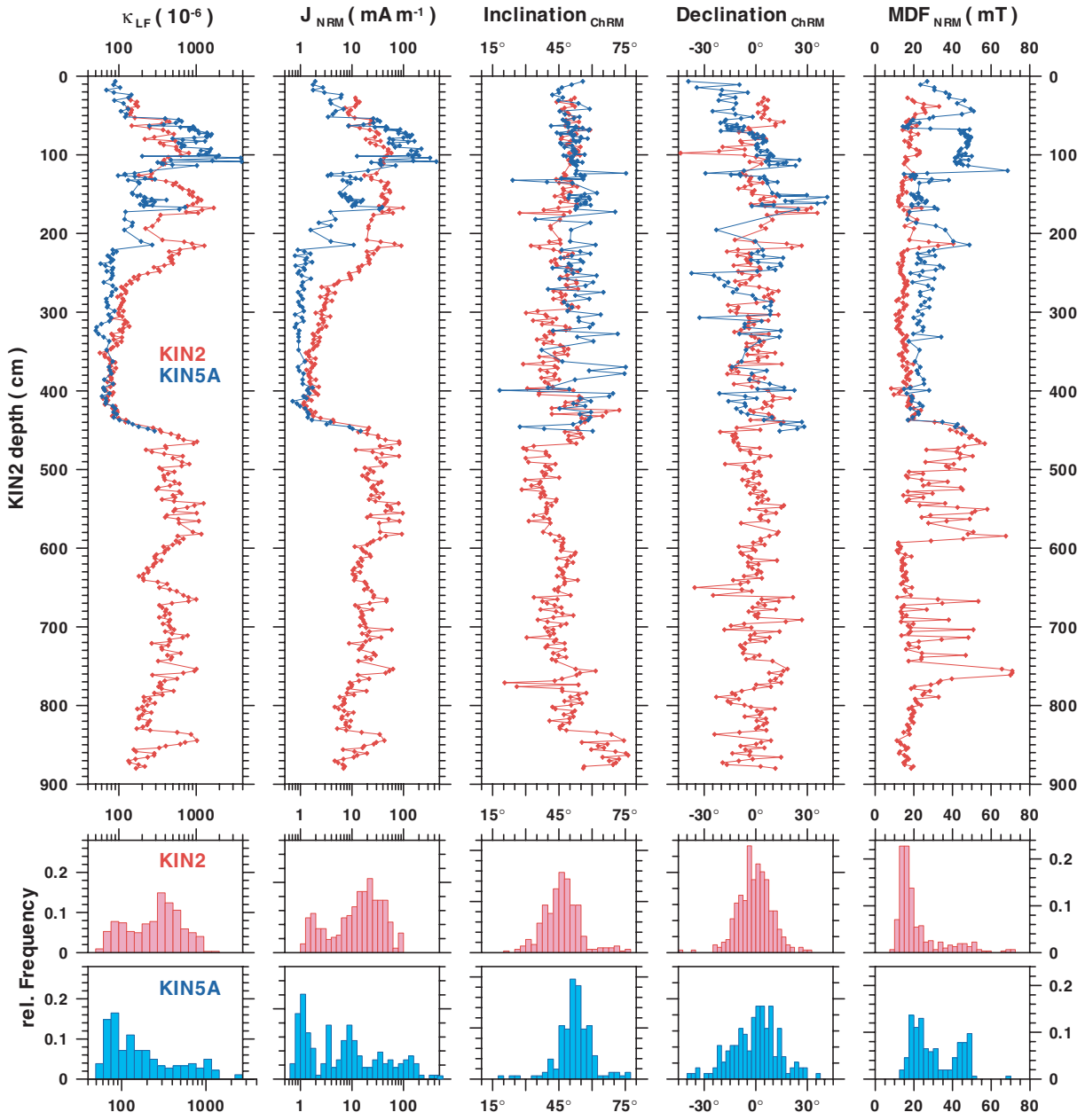

Figure 3. Down-core variations of paleomagnetic properties determined on discrete samples (from left to right): low-field bulk susceptibility (κ_{LF}), intensity of the natural remnant magnetization (J_{NRM}), inclination (and site inclination at 49°) and declination of the characteristic remanent magnetization (ChrM) isolated after AF demagnetization, Median Destructive Field (MDF_{NRM}) of NRM for cores KIN2 (red), as reference core, and KIN5A (blue). The relative frequencies of the individual properties and cores are shown in separate histograms at the bottom.

RESULTS

In the all figures, the data sets are plotted versus the depth scale of KIN2, according to the correlation shown in Fig. 2. Results from the shortest core KIN5 are very similar to the results from longer core KIN5A. Therefore, mainly data from core KIN5A are presented in most of the figures.

The down-core variations of five paleomagnetic properties from cores KIN2 and KIN5A are shown in Fig. 3, together with the respective histograms of their relative frequency. The low-field magnetic susceptibility (κ_{LF}) varies over two orders of magnitude from 50 to 4000 $\times$ 10^{-6}, whereas the intensity of NRM (J_{NRM}) covers nearly three orders of magnitude, from 0.7 to 500 mAm^{-1}, along the two cores. The ChRM inclinations and declinations are consistent with a geocentric axial dipole (GAD) field (GAD inclination = 54.4°), but they are characterized by a large scattering, which does not allow any correlation of the directional data. The MDF_{NRM} varies between 15 and 75 mT, indicating a wide spectrum of the grain size and/or mineralogy of remanence carriers. The overall similarity between the κ_{LF} and J_{NRM} implies that the NRM intensity is primarily controlled by concentration variations of magnetic particles. However, there are differences in concentration of about a factor of 10 within contemporaneous intervals (note the logarithmic scales) when comparing both cores. This demonstrates the ambiguity of correlation between cores KIN2 and KIN5A.

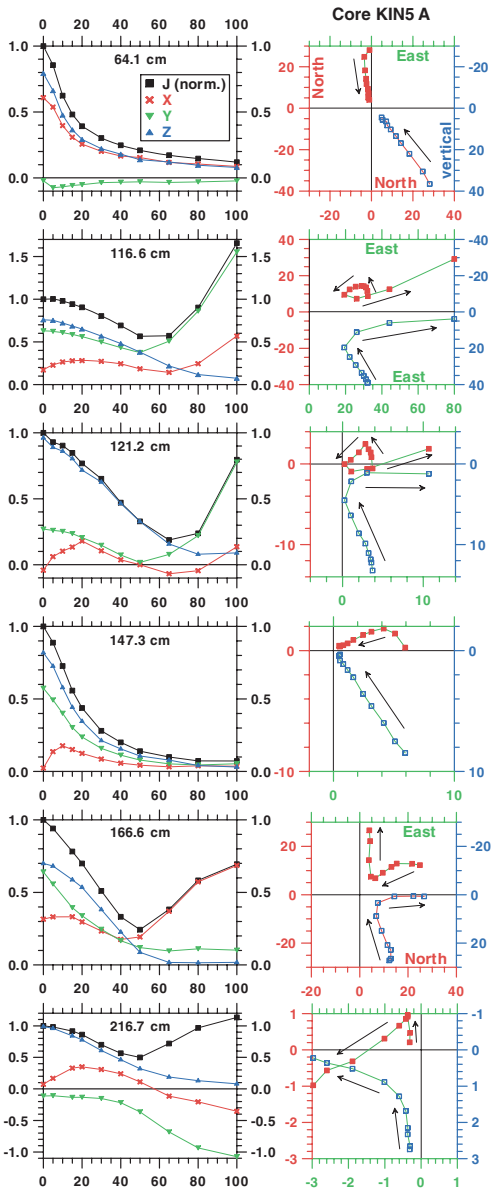

Figure 4. NRM-normalized demagnetization curves (left) of NRM intensity (black), as well as of the Cartesian components (X red, Y green, Z blue), and combined vector end point diagrams (right) of selected samples illustrating the various types of behaviour during AF demagnetization of NRM. Closed (open) symbols denote data in the horizontal (vertical) plane. Arrows point towards higher AF levels. Samples 116.6 cm, 121.2 cm, 166.6 cm and 216.7 cm show various degrees of GRM acquisition at high AF levels.

Figure 4 presents selected results of AF demagnetization of the NRM. Plots on the left show the behaviour of normalized NRM intensity (J/J_{NRM}) as well as the individual Cartesian components (in sample coordinates, also normalized by J_{NRM}) during AF experiments. All samples are from core KIN5A. The corresponding vector end point diagrams are shown on the right. Samples 116.6 cm, 121.2 cm, 166.6 cm and 285.5 cm begin to acquire a new magnetization at about 50 mT. It consequently shifts the vector end points away from the origin (indicated by arrows in Fig. 4) or even a swing around, such as in sample 121.2 cm. In the extreme cases of samples 116.6 cm and 216.7 cm, the NRM could not be reduced to less than 50 percent, hindering the calculation of the MDF_{NRM}. At 100 mT, sample 116.6 cm even gained a magnetization of about 1.7 times higher than the initial NRM intensity. The observed remanence acquisition during AF treatment is interpreted as a Gyro Remnant Magnetization (GRM), which is typical, and one indication for the presence of greigite (e.g. Snowball 1997; Stephenson & Snowball 2001). Therefore, additional experiments were performed to substantiate the presence of greigite. Samples 64.1 cm and 147.3 cm show the normal behaviour that expected during AF demagnetization (Fig. 4). The AF treatment removes a soft VRM component and finally reveals a stable magnetic vector of the samples all the way to 100 mT and the stable vector heading toward the origin.

Figure 5 shows the down-core results from some standard rock magnetic parameters. The MDF of the ARM (MDF_{ARM}), as a simple proxy of coercivity, the intensities of ARM (J_{ARM}) and SIRM (J_{SIRM}) as measures of magnetic concentration, the ratio between J_{SIRM} and κ_{LF} (J_{SIRM}/κ_{LF}), used to resolve between magnetite and greigite, and the *S*-ratio, generally used to estimate the presence of high-coercivity minerals (hematite/goethite) versus low-coercivity minerals (Magnetite/greigite). The similarity amongst J_{ARM} and J_{SIRM} (and also κ_{LF} and J_{NRM}, see Fig. 3) strongly indicates that their amplitudes are mostly controlled by concentration variations of magnetic particles, spanning three orders of magnitude. High J_{SIRM}/κ_{LF} ratios exceeding 30 kAm^{-1}, and reaching even more than 80 kAm^{-1} in the upper part of core KIN5A and in lower parts of core KIN2, are clear indications for the presence or even the dominance of greigite as remanence carrier. According to Maher *et al.* (1999), the SIRM of greigite lies between the SIRMs of 'soft' and 'hard' magnetite, but its magnetic susceptibility is lower by about a factor of 0.3 and less. Thus, values of $J_{SIRM}/\kappa_{LF} > 30$ kAm^{-1} can be indicative of greigite (see also Dekkers & Schoonen 1996).

The *S*-ratio parameter in cores KIN2 and KIN5A is commonly higher than 0.9, indicating that low-coercive minerals, such as magnetite and greigite control the magnetic properties. Intervals with *S*-ratios very close to 1 indicate that low-coercive carriers are the only magnetic carrier, such as seen in two longer segments of core KIN5A and parts of KIN2. The segments of highest *S*-ratios coincide with segments of high MDF values, both of NRM and ARM, and also with segments of high J_{SIRM}/κ_{LF} ratios (see Figs. 3 and 5). This will be discussed in more detail later on.

Figure 6 demonstrates that samples that acquire GRM during AF demagnetization of NRM also show unexpected results during the acquisition of ARM. First, the three samples selected for a special experiment were demagnetized with a separate 2G-Enterprises single-axis demagnetizer at 100 mT (stars at 0 mT in Fig. 6), which is also used for ARM acquisition. In a second step, the samples were subjected to the standard ARM acquisition process, that is, exposure to a static field of 0.05 mT, superimposed on an AF of 100 mT, parallel to the sample *z*-axes, increasing the sample magnetization as indicated by the dashed lines at 0 mT in Fig. 6. This should increase the intensity only along the *z*-component of the sample. We found that the sample acquire magnetization also perpendicular to the *z*-axis, especially in sample 116.6 cm, that acquire significant component along the *x*-axis. In this sample, the ARM *x*-component is about 50 percent of the ARM z-component. A similar but less prominent effect can be seen in sample 120.2 cm (*x* equal to 12 percent of *z*) and sample 125.2 (*x* equal to 3 percent of *z*). In these cases, the ARM acquisition significantly deviates from the applied field direction, which was parallel to the *z*-axis.

After ARM acquisition, the samples were stepwise demagnetized with fields of up to 250 mT using the single-axis demagnetizer. The single-axis demagnetizer operates in the time domain only. The

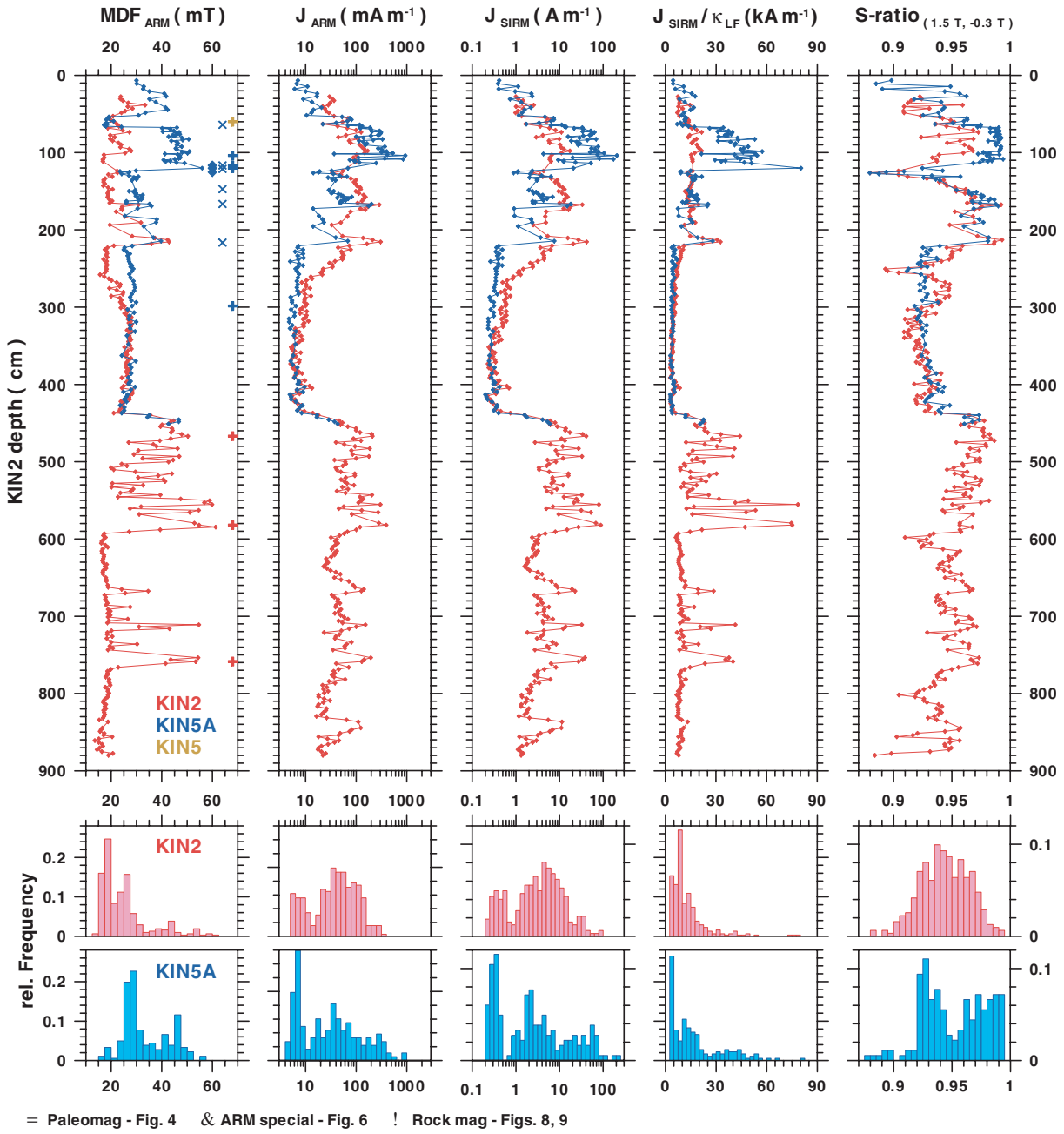

Figure 5. Down-core variations of rock magnetic properties of cores KIN2 (red) and KIN5A (blue), from left to right: median destructive field (MDF_{ARM}) and Intensity (J_{ARM}) of anhysteretic remnant magnetization, Intensity of saturated isothermal remnant magnetization (J_{SIRM}), ratio of SIRM intensity to low field susceptibility (J_{SIRM}/κ_{LF}) and *S*-ratio (for definition see text). The relative frequencies of the individual properties and cores are shown in separate histograms at the bottom.

sample rests in the coil centre and the field is ramped up and down with a constant rate. This was done in order to rule out possible instrumental artifacts.

In all three samples, the magnetization could be reduced with AF fields of 30 to 50 mT. However, the Cartesian components do not approach the field axis asymptotically, but overshoot after application of higher fields, 60 mT for the *x*-component and 95 mT for the *z*-component in sample 116.6 cm, and then acquire a new magnetization with opposite sign, continuously increasing until 250 mT. The *x*-component then was even larger than the initial value at 0 mT (after ARM acquisition). To test how the samples would react, they were again subjected to the ARM acquisition procedure (dashed lines at 250 mT in Fig. 6). In all three cases, the initial ARM values in all three components were reached again, including the acquisition of a remanence perpendicular to the applied field direction. This indicates that the selected samples are sensitive to the acquisition of a GRM during the ARM acquisition procedure too. In order to quantify this effect, we calculated the inclination of ARM in sample coordinates. Since the field was applied parallel to the *z*-axis, the ARM inclination should be 90°. When there is an acquisition of magnetization perpendicular to the applied field direction, the ARM inclination is lower, such as in sample 116.6 cm

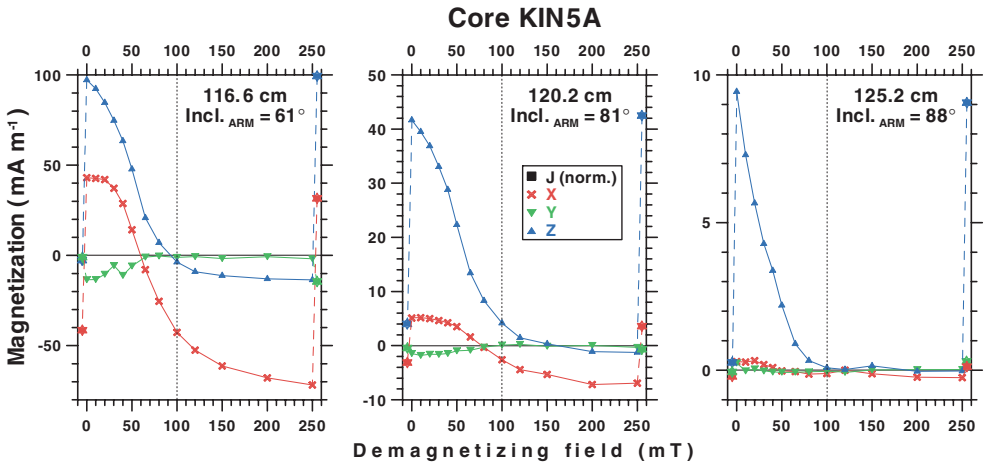

Figure 6. GRM acquisition of X, Y and Z component during acquisition of ARM and successive AF demagnetization of three selected sampled. Basically, the samples shown cannot be demagnetized properly with the application of alternating fields (for further details see text).

with an ARM inclination of only 61°. Thus the ARM inclination can be used to detect the presence of remanence carriers susceptible to GRM acquisition during ARM acquisition experiments.

Another significant conclusion from this experiment is that greigite bearing samples (Fig. 6) cannot be demagnetized properly with the AF method. Instead, they start to acquire a new magnetization when subjected to fields of 30 mT and higher (see also Fig. 4, sample 216.7 cm). Thus, in many cases, this effect could not have been identified during conventional single step AF demagnetization, for example, 20 mT demagnetization. The vertical dotted lines in Fig. 6 mark the 100 mT demagnetization level. Interestingly, during AF treatment of the imprinted ARM, the individual components cross this line at a magnetization level measured after the initial AF demagnetization, and before imprinting the ARM. This means that the gyro remnant effect is mainly due to the AF acting on the remanence carriers. It is consistent with the observation that during demagnetization of the NRM, an acquisition of a GRM was also observed in numerous samples when they were subjected to fields of 50 mT and higher (see Fig. 4). In contrast to this finding, no significant acquisition of a GRM could be observed during IRM acquisition which was performed with unidirectional-pulse fields.

Figure 7 shows compilation of the rock magnetic properties indicative to the presence of greigite in cores KIN2, KIN5 and KIN5A. As pointed out, the ratio of J_{SIRM}/κ_{LF}, is the most significant parameter. Samples where this ratio exceed the magnetite background of about 10 kAm^{-1} obviously contain a significant amount of greigite, with J_{SIRM}/κ_{LF} ratios reaching up to 80 kAm^{-1}. In such cases, significant deviation of the acquired ARM direction from the applied field direction can be observed with ARM inclination values lower than 90° and that can reach values as low as 60°. However, the correlation between high J_{SIRM}/κ_{LF} ratios and low ARM inclinations seems to be not linear. A similarity can also observed between the curves of J_{SIRM}/κ_{LF} and κ_{ARM}/κ_{LF}. For pure magnetite assemblages, the ratio κ_{ARM}/κ_{LF} can be used as a grain-size indicator (King *et al.* 1982) with low (high) values indicating large (small) grain sizes of magnetite. According to Maher *et al.* (1999), (Table 1.2), the ratio ARM/κ_{LF}, and κ_{ARM}/κ_{LF}, are 3 and 30 times larger, respectively, for greigite, when compared to hard (soft) magnetite.

Figure 7 shows the AM_S represented by the degree of AM_S, as calculated by the ratio 100 $(K_{max}-K_{min})/K_{max}$, and the shape of the anisotropy ellipsoid, represented by the ratio $(K_{max}\cdot K_{min})/K^2_{int}$. In some intervals, where the susceptibility is nearly isotropic, e.g. $100\cdot(K_{max}-K_{min})/K_{max} = 0$ and $(K_{max}\cdot K_{min})/K^2_{int} = 1$, the alignment of magnetic grains is probably not controlled by depositional processes, but rather by crystal growth within the sediment (e.g. 500 cm and 580 cm in KIN2). This clearly suggests that greigite is a secondary mineral that results in a CRM. In KIN2, the degree of AM_S is lower and the anisotropy ellipsoid is less oblate relative to neighbouring sediments. Here, both magnetite, carrying DRM, and greigite, carrying a CRM, should be present. Most isotropic horizons or horizons of significantly lower anisotropy (relative to neighboring samples) coincide with increased ratios of κ_{ARM}/κ_{LF}, lowered ARM inclination and high J_{SIRM}/κ_{LF}. However, the interparameter correlation is again not straightforward.

The large variability in concentration covering three orders of magnitude (Figs. 3 and 5) and composition of magnetic carriers, Ti-magnetite, greigite, or both in varying ratio (Fig. 7) suggest that the recovered sediments from Lake Kinneret are not adequate for relative paleointensity measurements. Therefore, we do not present any results or attempt to reconstruct a relative paleointensity record.

Figure 8 summarizes the behaviour of selected samples during AF demagnetization of NRM, thermomagnetic experiments, IRM acquisition, and hysteresis experiments. Samples KIN5A-103.7 cm, KIN5A-116.6 cm and KIN2-582.0 cm that have a high MDF_{NRM} and/or show a GRM acquisition, exhibit significant and irreversible intensity drop between 300 °C and 400 °C during thermomagnetic measurements and are also characterized by a narrow field range of IRM acquisition and a wide hysteresis loop. The combination of these properties is an unequivocal indication that greigite dominates the sediment magnetism, even though they also contain some magnetite. This is evident by the thermomagnetic experiments that show a second intensity drop at about 580 °C. In contrast, samples KIN5-60.1 cm, KIN5A-298.4 cm and KIN2-758.5 cm show that magnetic properties are dominated by magnetite, although varying amounts of greigite are also present, as can be seen in the thermomagnetic behaviour. In all cases, greigite is destroyed and new magnetite is formed during heating. The narrow coercivity spectra of greigite-dominated samples explain why they also show *S*-ratios very close to 1 as usually observed for magnetite bearing rocks. In Lake Kinneret cores, however, high *S*-ratio values seem to be typical of greigite bearing sediments. This possibly indicates that the 'hard' components of magnetization as carried by antiferromagnetic iron

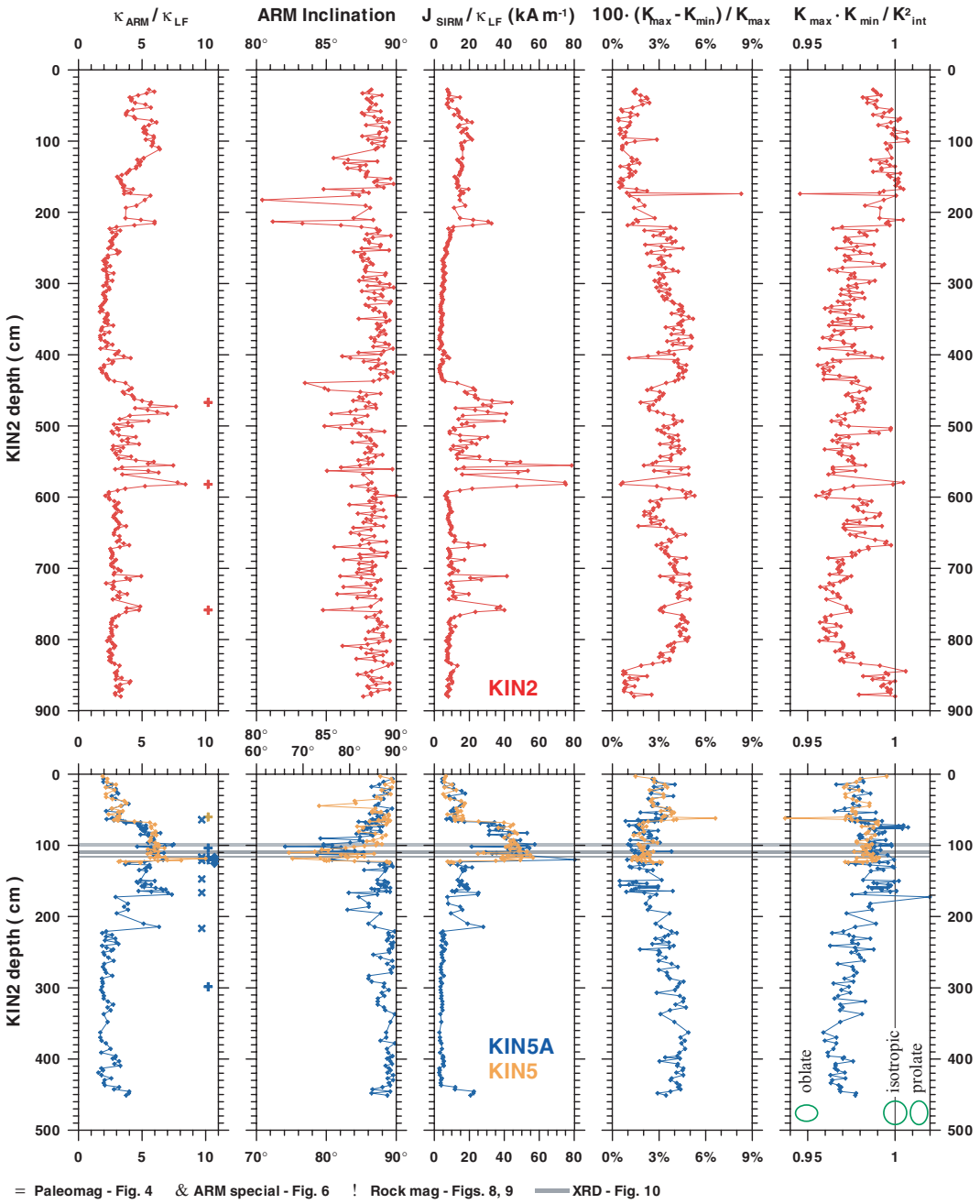

Figure 7. Down-core variations of the susceptibility ratio κ_{ARM}/κ_{LF} (κ_{ARM} = anhysteretic susceptibility), ARM inclination as a measure of GRM acquisition, J_{SIRM}/κ_{LF} as a proxy for greigite concentration and degree of the anisotropy of magnetic susceptibility (AM_S) measured by the ratio $100\cdot(K_{max}-K_{min})/K_{max}$, and the shape of the anisotropy ellipsoid measured by the ratio $(K_{max}\cdot K_{min})/K^2_{int}$.

mineral phases, such as hematite or goethite are not present in the reducing greigite forming environment.

Figure 9 presents the domain state of 19 samples, and for eight of them, the corresponding thermomagnetic results. From several samples, we extract separately dark or bright layers in order to test if there is difference between the two. It is apparent that samples that show a significant intensity drop between 300° and 400 °C, indicating the dominance of greigite, also show single domain (SD) like behavior, in contrast, samples with a significant (additional) intensity drop at 580°C, indicating the presence of magnetite, show pseudo-single domain (PSD) like behaviour. Roberts (1995) observed similar hysteresis results for greigite, yet he stated that SD greigite is related to larger grain size when compared to SD magnetite. Thus, Fig. 9 should not be interpreted directly in term of grain size.

Figure 10 shows the diffractograms of the four magnetic extracts, together with the corresponding thermomagnetic curves. Results from the Rietveld *et al.* (1998) mineral analysis are listed in Table 1. The extracts, which are all black, are clearly dominated by greigite, that is about 10 times more abundant than Ti-magnetite. Only in sample four, the ratio is lower, about 4:1. The magnetic extracts also contain some nonmagnetic minerals, mainly calcite, pyrite, quartz

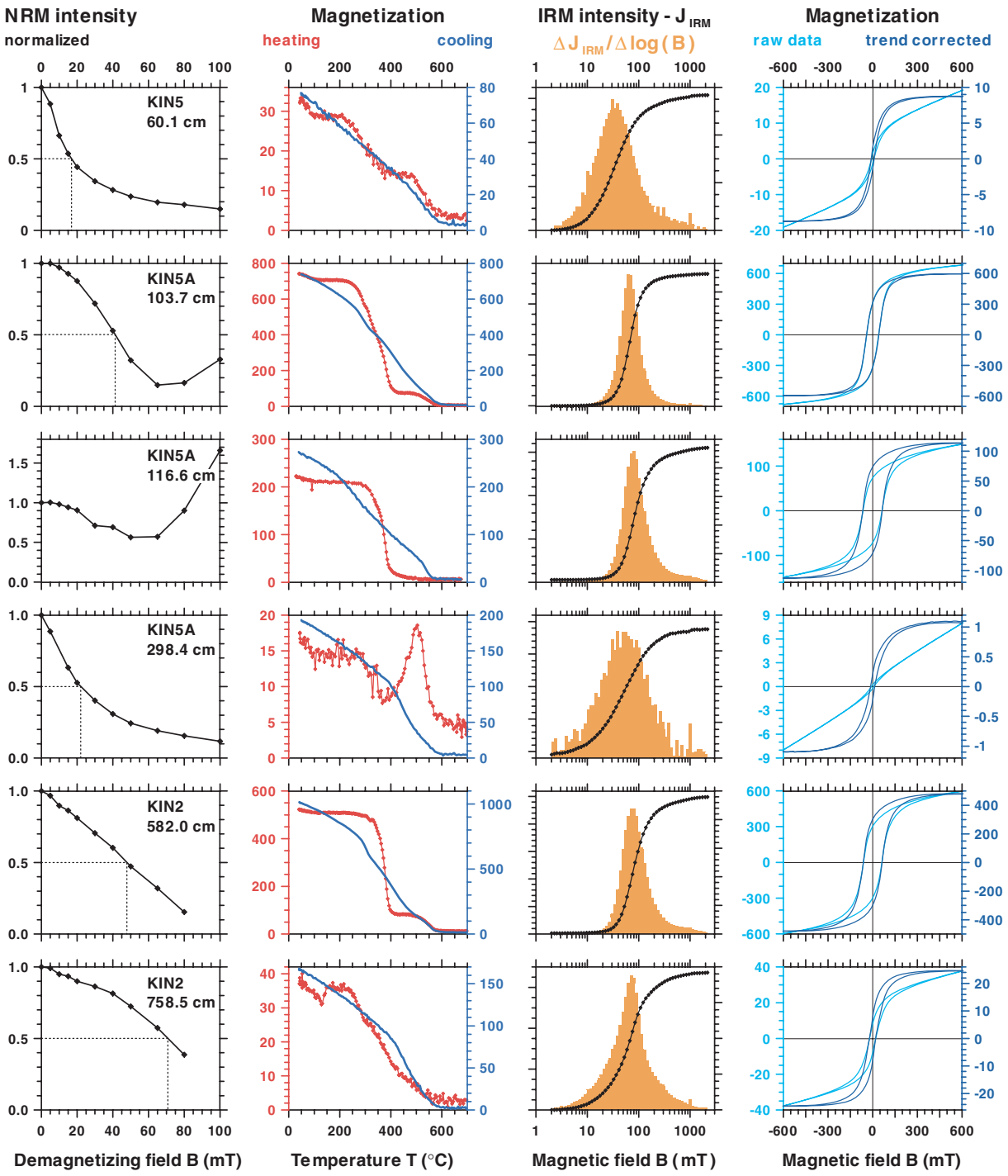

Figure 8. Selected samples from Lake Kinneret demonstrating the variable paleo- and rock magnetic properties (from left to right): normalized NRM demagnetization curves with the dotted lines indicating the median destructive field (MDF_{NRM}), thermomagnetic curves with separate axes for heating (red) and cooling (blue), IRM acquisition (black) and log IRM acquisition rates (orange), both in arbitrary units and hysteresis loops, light blue – raw data, dark blue – slope corrected for paramagnetic contribution; magnetization in arbitrary units.

and sulphur that showed up with the greigite. The greigite and pyrite are probably forming intergrowth aggregates due to the transformation of polysulphide to monosulphide.

The thermomagnetic curves of the extracts clearly show the dominance of greigite in the heating curve, completely disintegrating between about 250 and 400°C. This confirms independently the XRD results. The smaller amount of magnetite present in the samples, as derived from XRD analyses, can be recognized also from its Curie temperature of around 580 °C. Although the thermomagnetic curves were obtained in an argon atmosphere, additional magnetite is formed in samples two and four during cooling from 700°C, even exceeding the initial magnetization (note the different

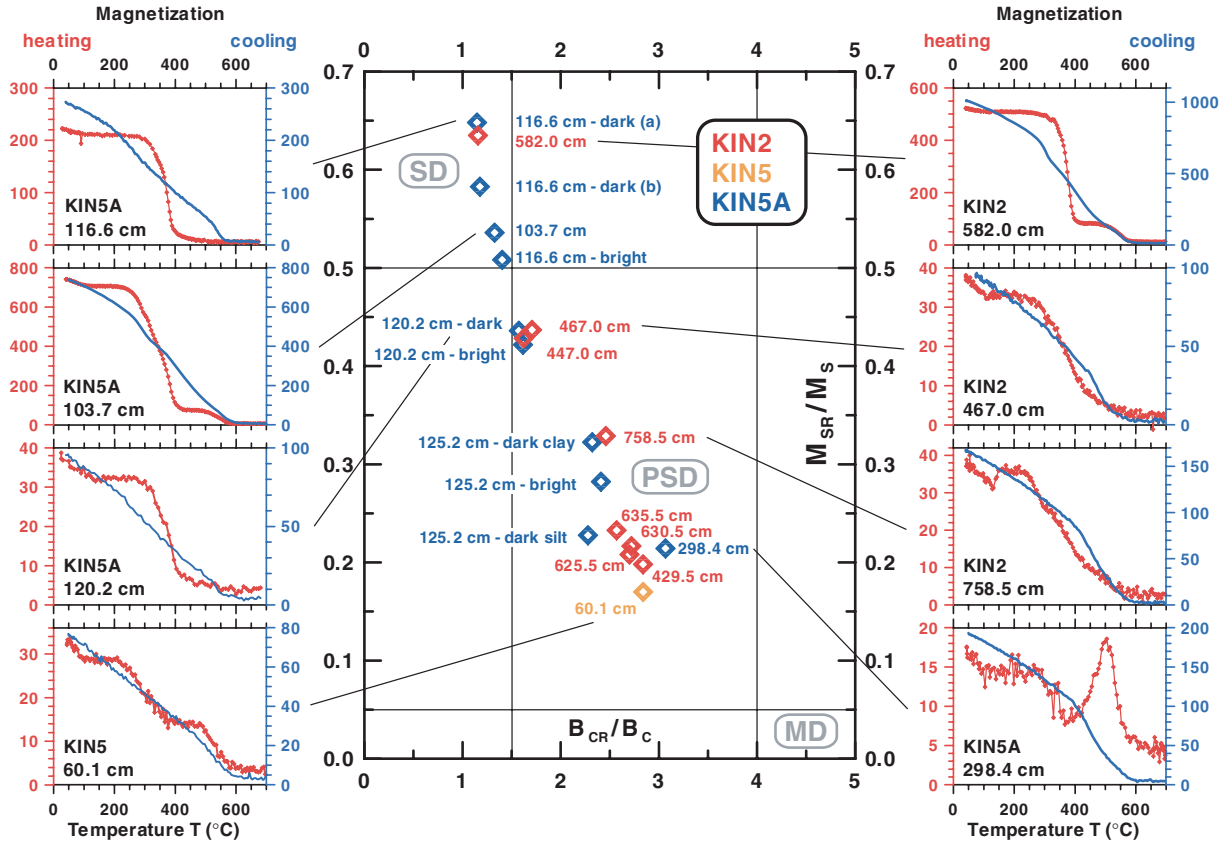

Figure 9. Combination of domain state and thermomagnetic properties of selected subsamples from Lake Kinneret cores, revealing the single domain (SD) like behaviour of greigite, superimposed to varying degrees on the pseudo-single domain (PSD) behaviour of magnetites. Note the partly different axis scaling for the heating (red) and cooling (blue) curves.

axis scales). The remaining magnetization in samples one and three is less when compared to the initial values.

DISCUSSION AND CONCLUSIONS

The main result of our study is that magnetizations of late Pleistocene sediments recovered from Lake Kinneret is carried by strong CRM, dominated by single-domain (SD) greigite, superimposed on a DRM, carried by pseudo-SD (PSD) magnetite. Other studies on marine and lake sediments report similar findings, (Roberts & Turner 1993; Hallam & Maher 1994; Roberts 1995; Sagnotti & Winkler 1999; Jelinowska *et al.* 1999; Ron *et al.* 2006).

Greigite, as a diagenetic iron sulphide precipitate can be detected in sediments using a combination of simple rock magnetic experiments (Snowball 1991; Roberts 1995; 1997). We have demonstrated the usefulness of: (1) the ratio J_{SIRM}/κ_{LF} (high values of 30 to 80 kAm^{-1}); (2) high MDF of NRM and ARM (30 to 70 mT); (3) acquisition of a GRM during AF treatment of NRM from about 30 to 50 mT on; (4) the ARM direction deviating from the applied field direction, as monitored by ARM inclinations $< 90°$; (5) hysteresis parameters indicating SD like behaviour; (6) the narrow field range of IRM acquisition; (7) the irreversible collapse of magnetization between 300° and 400°C during thermomagnetic measurements and (8) *S*-ratios very close to 1.0.

Our study shows that CRM acquisition is the dominant magnetization processes in late Pleistocene Lake Kinneret sediments (Fig. 3). Due to large amounts of greigite, the studied sediments are probably not faithful recorders of the geomagnetic field. Hence, interpretation of paleomagnetic record obtained from greigite bearing sediments, in general, should be exercised with caution because:

(1) Records of geomagnetic secular variations can be biased due to a large coercivity overlap between primary magnetite and secondary greigite, consequently, their relative contributions to the NRM cannot be separated by AF demagnetization.

(2) AF demagnetization of greigite often produces vector distortions by acquisition of GRM at the same AF levels.

(3) Estimation of relative paleointensity can be hampered by large-scale variations in NRM intensity due to the acquisition of a secondary CRM of unknown age and unknown extent superimposed on the DRM. Furthermore, the intensity of ferrimagnetic CRM is usually higher when compared to DRM intensity carried by same amount of carrier. This is because magnetic moment alignment is more effective during growth of magnetic minerals than during deposition of magnetic particles.

Nevertheless, according to Hallam & Maher (1994) greigite bearing sediments still might be useful for reconstruction of polarity records since the epigenetic processes are shorter than 10^3 yr. Recently, however, Roberts *et al.* (2005); Roberts & Weaver (2005) and Sagnotti *et al.* (2005) show that CRM processes can be much longer and very complex and even alter the polarity sequence of the sediments.

The precipitation of greigite requires reducing conditions at the sediment–water interface and/or interstitial water, associated with the presence of sulphur and iron oxides. Reducing conditions are

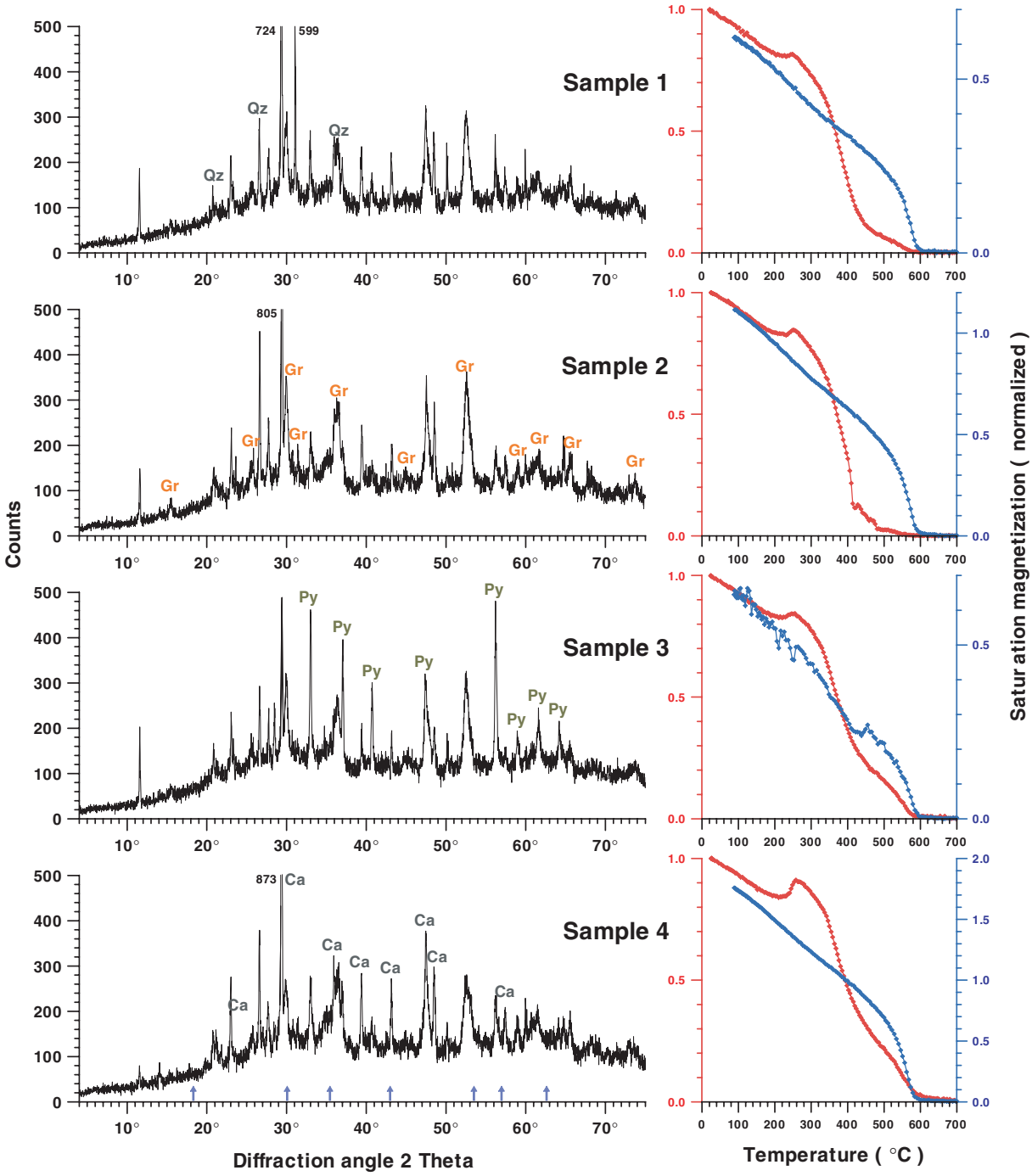

Figure 10. X-ray diffraction (XRD) data of four magnetic extracts from Core KIN5A (see also Table 1) and corresponding thermomagnetic curves, illustrating the dominance of greigite as the magnetic carrier mineral in the investigated samples. Numbers in the XRD data indicate amplitudes exceeding the axis scaling. For reasons of clarity, the main minerals occurring in the extracts are indicated on different graphs: Qz – quartz, Gr – greigite, Py – pyrite, Ca – calcite. Blue arrows indicate the positions where magnetite peaks would be visible.

achieved in and are typical of stratified lakes and other stratified water bodies, such as the Dead Sea, paleo-Lake Lisan, temporarily the Eastern Mediterranean Sea, the Caspian Sea, the Black Sea and many other marine basins. The down-core variations of magnetic concentration may point to time intervals when the lake was not stratified (interval 3 to 4.30 in KIN2), recognized from low J_{SIRM}/κ_{LF} ratios, low MDF and low susceptibility, hence indicating the absence of greigite, or rapid fluctuation between the two states (interval 4.30 to 6 m in KIN2). It may imply long- or short-term fluctuations in fresh water supply to the lake that suppresses the stratification and by inference rainy or dryer periods. Previous secular variations data from lake Kinneret reported by Thompson *et al.* (1984) should be carefully treated and cannot be taken as a reference curve. Marco (2002) also presented paleomagnetic results from a trench very close by the site of the cores of this study without any rock magnetic data. Therefore, the postulated record of

a geomagnetic excursion leaves some doubts, since the investigated cores covering the same stratigraphic sequence could not confirm it.

It is possible that the presence of greigite in lake sediments and closed basins has been overlooked in the past in other studies where no rock magnetic data were acquired. By and large, we infer that a lack of rock magnetic data may result in erroneous interpretation of paleomagnetic records from lake sediments, and that paleomagnetic record from anoxic sedimentary environment, in general, should be treated with caution.

ACKNOWLEDGMENTS

We would like to acknowledge the following people for technical support and help during the drilling campaign D. Acksel, C. Brüchmann and T. Kulbe, N. Hazan, E. Ram and M. Golan. M. Duwe and M. Haack helped during sampling for paleo- and rock magnetic investigations. Financial support was provided by the HGF Strategiefondsprojekt KIHZ (Klima in historischen Zeiten/Natural Climate Variations from 10,000 years to the present day). Thanks to D. Williamson and I. Snowball for their reviews and comments which helped us improve the manuscript.

REFERENCES

Bartov, Y., Stein, M., Enzel, Y., Agnon, A. & Reches, Z., 2002. Lake-levels and sequence stratigraphy of lake Lisan, the late pleistocene precursor of the Dead Sea, *Quate. Res.,* **57,** 9–21.

Begin, Z.B., Broccker, B., Buchbinder, B., Druckmann, Y., Kaufman, A., Magaritz, M. & Neev, D., 1985. Dead Sea and Lake Lisan levels in the last 30,000 years, *Geological Survey of Israel Bulletin,* **85,** 1–81.

Bergmann, J., Friedel, P. & Kleeberg, R., 1998. BGMN – a new fundamental parameters based Rietveld program for laboratory X-ray sources, it's use in quantitative analysis and structure investigations, Commission of Powder Diffraction, *Int. Union Crystallogr., CPD Newsletter,* **20,** 5–8.

Brachfeld, S.A. & Banerjee, S.K., 2000. A new high-resolution geomagnetic relative paleointensity record for the North American Holocene: A comparison of sedimentary and absolute intensity data, *J. Geophys. Res.,* **105,** 821–834.

Creer, K.M. & Morris, A., 1996. Proxy-climate and geomagnetic palaeointensity records extending back to ca. 75,000 BP derived from sediments cored from Lago Grande Di Monticchio, southern Italy, *Quat. Sci. Rev.,* **15,** 167–188.

Dekkers, M.J. & Schoonen, M.A.A., 1996. Magnetic properties of hydrothermally synthesized greigite (Fe3S4) – I. Rock magnetic parameters at room temperature. *Geopyhs. J. Int.,* **126**, 360–368.

Frank, U., Schwab, M.J. & Negendank, J.F.W., 2002. A lacustrine record of paleomagnetic secular variations from Birkat Ram, Golan Heights (Israel) for the last 4400 years, *Phys. Earth Planet. Inter.,* **133,** 21–34.

Frank, U., Schwab, M.J. & Negendank, J.F.W., 2003. Results of rock magnetic investigations and relative paleointensity determinations on lacustrine sediments from Birkat Ram, Golan Heights (Israel), *J. Geophys. Res.,* **108**(B8), 2379. doi: 10.1029/2002JB002049.

Hallam, D.F. & Maher, B.A., 1994. A record of reversed polarity carried by iron sulphide greigite in the British early Pleistocene sediments, *Earth Planet. Sci. Lett.*, **121**, 71–80.

Hazan, N., Stein, M., Agnon, A., Marco, S., Nadael, D., Negendank, J.F.W., Schwab, M.J. & Neev, D., 2005. The late quaternary limnology history of Lake Kinneret (Sea of Galilee, Israel), *Quater. Res.,* **63,** 60–77.

Jelinowska, A., Tucholka, P. & Badaut-Trauth, D., 1999. Magnetic mineral variations of south Caspian Sea sediments at laminae scale, *Phys. Chem. Earth (A),* **24**(9), 823–828.

Kawai, N., Nakajima, T., Yaskawa, K., Torii, M. & Natsuhara N., 1975. Palaeomagnetism of Lake Biwa sediment, *Rock Mag. Palaeogeophys.,* **3,** 24–31.

King, J.W., Banerjee, S.K. & Marvin J., 1983. A new rock-magnetic approach to selecting sediments for geomagnetic palaeointensity studies: Application to palaeointensity for the last 4000 yr, *J. Geophys. Res.,* **88,** 5911–5921.

King, J.W., Banerjee, S.K., Marvin, J. & Özdemir, Ö., 1982. A comparison of different magnetic methods for determining the relative grain size of magnetite in natural materials: some results from lake sediments, *Earth Planet. Sci. Lett.,* **59,** 404–419.

Kirschvink, J.L., 1980. The least-squares line and plane and the analysis of palaeomagnetic data, *Geophys. J. R. Astr. Soc.,* **62,** 699–718.

Maher, B., Thompson, R. & Hounslow, M.W., 1999. *Introduction to 'Quaternary climates, environments and magnetism',* Maher, B. & Thompson, R. (eds.), Cambridge University Press, Cambridge, pp. 1–48.

Marco, S., Ron, H., McWilliams, M.O. & Stein, M., 1998. High-resolution record of geomagnetic secular variation from late Pleistocene Lake Lisan Sediments (Paleo Dead Sea). *Earth Planet. Sci. Lett.,* **161,** 145–160.

Marco, S., Ron, H., McWilliams, M.O. & Stein M., 1999. The locking in of remanence in Late Pleistocene sediments of Lake Lisan (palaeo Dead Sea), *Geol. Soc. London Spec. Publ.,* **151,** 47–52.

Marco, S., 2002. Late Pleistocene paleomagnetic secular variation from the Sea of Galilee, Israel, *Geophy. Res. Lett.,* **29**(21), 2015, doi:10.1029/2001GL014038.

Nowaczyk, N.R., 2001. Logging of magnetic susceptibility, in: W.M. Last & J.P. Smol (eds.), *Tracking Environmental Changes in Lake Sediments: Basin Analysis, Coring, and Chronological Techniques,* Kluwer Academic Publishers, Dordrecht, Netherlands, pp. 155–170.

Nowaczyk, N.R., 2003. Detailed study on the anisotropy of magnetic susceptibility of arctic marine sediments. *Geophys. J. Int.,* **152,** 302–317.

Nowaczyk, N.R., Harwart, S. & Melles, M., 2000. A rock magnetic record from Lama Lake, Taymyr Peninsula, northern Central Siberia. *J. Paleolimnol.,* **23**(3), 227–241.

Nowaczyk, N.R. *et al.*, 2002. Magnetostratigraphic results from impact crater Lake El'gygytgyn, northeastern Siberia: a 300 kyr long high-resolution terrestrial palaeoclimatic record from the Arctic, *Geophys. J. Int.,* **150,** 109–126.

Peck, J.A., King, J.W., Colman, S.M. & Kravchinsky, V.A., 1996. An 84-kyr paleomagnetic record from the sediments of Lake Baikal, Siberia, *J. Geophys. Res.,* **101,** 11,365–11,385.

Roberts, A.P., 1995. Magnetic properties of sedimentary greigite (Fe3S4), *Earth Planet. Sci. Lett.,* **134,** 227–236.

Roberts, A.P. & Turner, G.M., 1993. Diagenetic formation of ferromagnetic iron sulphide minerals in rapidly deposited marine sediments, South Island, New Zealand, *Earth Planet. Sci. Lett.,* **115,** 247–273.

Roberts, A.P., Jiang, W.-T., Florindo, F., Horng, C.-S. & Laj, C., 2005. Assessing the timing of greigite formation and the reliability of the Upper Olduvai polarity transition record from the Crostolo River, Italy, *Geophy. Rese. Lett.,* **32,** doi: 10.1029/2004GL022137.

Roberts, A.P. & Weaver, R., 2005. Multiple mechanisms of remagnetization involving sedimentary greigite (Fe3S4), *Earth Planet. Sci. Lett.,* **231,** 263–277.

Ron, H., Nowaczyk, N.R., Frank, U., Marco, S. & Mcwilliams, M.O., 2006. Magnetic properties of Lake Lisan and Holocene Dead Sea sediments and the fidelity of chemical and detrital remanent magnetization, in: Enzel, Y., Agnon, A. & Stein, M. (eds), *GSA book new frontiers in Dead Sea paleoenvironmental research,* GSA Special Paper 401, pp. 171–182.

Sagnotti, L. & Winkler, A., 1999. Rock magnetisem and paleomagnetisem of greigite-bearing mudstone in the Italian peninsula, *Earth Planet. Sci. Lett.,* **165,** 67–80.

Sagnotti, L., Roberts, A.P., Weaver, R., Verosub, K.L., Florindo, F., Pike, C.R., Clayton, T. & Wilson, G.S., 2005. Apparent magnetic polarity reversals due to remagnetization resulting from late diagenetic growth of greigite from siderite, *Geophys. J. Int.,* **160,** 89–100, doi:10.1111/j.1365-246X.2005.02485.x.

Schwab, M.J., Neumann, F., Litt, T., Negendank, J.F.W. & Stein, M., 2004. Holocene paleoecology of the Golan Heights (Near East): investigation of lacustrine sediments from Birkat Ram crater lake, *Quat. Sci. Rev.,* **23,** 1723–1731.

Snowball, I., 1991. Magnetic hysteresis properties of greigite (Fe3S4) and a new occurrence in Holocene sediments from Swedish Lappland, *Phys. Earth Planet. Inter.,* **68,** 32–40.

Snowball, I., 1997. Gyroremanent magnetization and the magnetic properties of greigite-bearing clays in southern Sweden, *Geophys. J. Int.,* **129,** 624–636.

Stein, M., 2001. The sedimentary and geochemical record of Neogene Quaternary water bodies in the Dead Sea basin — inference for the regional paleoclimatic history, *J. Paleolimnol.,* **26,** 271–287.

Stephenson, A. & Snowball, I., 2001. A large gyromagnetic effect in greigite. *Geophys. J. Int.,* **145,** 570–575.

Tauxe, L., 1993. Sedimentary records of relative paleointensity of the geomagnetic field: Theory and practice, *Rev. Geophys.,* **31,** 319–354.

Thompson, R., Turner, G.M., Stiller, M. & Kaufman, A., 1984. Near East paleomagnetic secular variation recorded in sediments from the Sea of Galilee (Lake Kinneret), *Quat.. Res.,* **23,** 175–188.

Thouveny, N., Creer, K.M. & Williamson, D., 1993. Geomagnetic moment variations in the last 70,000 yr, impact on production of cosmogenic isotopes, *Global Planet. Change,* **7,** 157–172.

Williams, T., Thouveny, N. & Creer, K.M., 1998. A normalised intensity record from Lac du Bouchet: Geomagnetic palaeointensity for the last 300 kyr? *Earth Planet. Sci. Lett.,* **156,** 33–46.